Spatio-temporal modelling of PM_{10} daily concentrations in Italy using the SPDE approach

Guido Fioravanti[a,*], Sara Martino[b], Michela Cameletti[c], Giorgio Cattani[a]

[a] *a) Italian National Institute for Environmental Protection and Research, Department for environmental evaluation, control and sustainability. Via Vitaliano Brancati 48, 00144 Rome, Italy*
[b] *Norwegian University of Science and Technology, Trondheim, Norway*
[c] *University of Bergamo, Bergamo, Italy*

Abstract

This paper illustrates the main results of a spatio-temporal interpolation process of PM_{10} concentrations at daily resolution using a set of 410 monitoring sites, distributed throughout the Italian territory, for the year 2015. The interpolation process is based on a Bayesian hierarchical model where the spatial-component is represented through the Stochastic Partial Differential Equation (SPDE) approach with a lag-1 temporal autoregressive component (AR1). Inference is performed through the Integrated Nested Laplace Approximation (INLA). Our model includes 11 spatial and spatio-temporal predictors, including meteorological variables and Aerosol Optical Depth. As the predictors' impact varies across months, the regression is based on 12 monthly models with the same set of covariates. The predictive model performance has been analyzed using a cross-validation study. Our results show that the predicted and the observed values are well in accordance (correlation range: $0.79 - 0.91$; bias: $0.22 - 1.07$ $\mu g/m^3$; RMSE: $4.9 - 13.9$ $\mu g/m^3$). The model final output is a set of 365 gridded ($1km \times 1km$) daily PM_{10} maps over Italy equipped with an uncertainty measure. The spatial prediction performance shows that the interpolation procedure is able to reproduce the large scale data features without unrealistic artifacts in the generated PM_{10} surfaces. The paper presents also two illustrative examples

*Corresponding author
Email address: `guido.fioravanti@isprambiente.it` (Guido Fioravanti)

of practical applications of our model, exceedance probability and population exposure maps.

Keywords: particulate matter, Bayesian hierarchical model, GRF, INLA, GMRF, exceedance probability, exposure map

---

1. Introduction

Worldwide, exposure to single pollutants (such as particulate matter, ozone, nitrogen dioxide) accounts for a large portion of overall mortality and cardio-respiratory morbidity (EEA, 2019). Accordingly, air pollution is recognized as a major public health issue. Among pollutants, particulate matter (PM) is the one associated most consistently with a variety of adverse health outcomes (Martuzzi et al., 2006; Langanke, 2015), even at very low concentrations (Piscitelli et al., 2019). WHO (2013) provides a review of the scientific literature concerning the impacts of air pollutants exposure on human health, while Samoli et al. (2013) investigates the adverse health effect of coarse (PM_{10}) and fine ($PM_{2.5}$) particulate matter in ten Mediterranean metropolitan areas. In particular, for a 10 $\mu g/m^3$ increase in $PM_{2.5}$ concentrations on the day of the death and the previous one (lag 0-1), a 0.55%, 0.57% and 0.72% increase was estimated in all-cause, cardiovascular and respiratory mortality, respectively. In addition, PM_{10} was positively associated with all-cause mortality at lag 0-1 and to cardiovascular and respiratory mortality for longer periods of cumulative exposure (lag 0-5).

In the European context, Italy sadly boasts some of the worst cities and areas for air pollution. The Po Valley in the North of Italy is one of the largest European regions of particular concern in terms of air quality (Raffaelli et al., 2020): high and widespread emissions, along with peculiar orographic and meteorological conditions favour both stagnation and formation of secondary particles in winter, and photochemical smog events in summer (EEA, 2019). Frequent PM_{10} daily limits exceedances are also recorded in south central Italy in the Sacco Valley (ISPRA, 2020) and the large Naples-Caserta agglomeration during winter months (De Marco et al., 2018).

Over the last decades Italy has recorded an important decrease in pollutant emissions thanks to more stringent measures undertaken in order to meet the targets set by the National Emission Ceilings Directive (Directive 2001/81/EC; EU, 2001). Significant PM_{10}, $PM_{2.5}$ and NO_2 downward trends have been recorded over large portion of the national monitoring network (ISPRA, 2019). Nonetheless, exceedances of the PM_{10} daily limit value of 50 $\mu g/m^3$ (not to be exceeded more than 35 days a year) and ozone long-term target value of 120 $\mu g/m^3$ still remain a problem in many cities and rural areas of the country.

Understanding how PM_{10} concentrations vary in both space and time is fundamental for a proper assessment of population-wide exposure and to formulate appropriate pollution mitigation strategies (Chu et al., 2015). While daily resolution for PM_{10} concentrations is often sufficient for exposure assessments, on the spatial scale, there has been an increasing need of high-resolution maps on large domains, in order to capture concentrations gradients both on the local and the national scale (Cohen et al., 2017). To this purpose, spatio-temporal statistical models have rapidly gained attention in the air quality scientific community (Hoek, 2017). The reason is that, compared to regional scale deterministic models, statistical models are generally easier to implement, require medium sized computing resources and provide higher resolution spatial predictions (Shahraiyni & Sodoudi, 2016).

In the statistical literature, the problem of building spatially continuous concentrations maps over large domains has been approached by different angles. A popular approach is that of Linear Mixed Models (LMM) which combine the possibility to include complex correlation structures, via easy-to-specify random effects at a low computational cost (Galecki & Burzykowski, 2013). LMM can in fact be easily implemented in a frequentist framework, using, among others, the popular `R` package `nlme` (Pinheiro et al., 2020). The use of LMM with regional random effects in the air quality community is reported in recent studies such as Kloog et al. (2015) and Stafoggia et al. (2017). One drawback of this methodology is that spatial dependence is expressed through discrete random effects that are related to geographic defined areas, resulting in prediction maps with spatial artifact (i.e. slabs), e.g. Sarafian et al. (2019) or Zhang et al. (2018). In addition, LMM do not incorporate, in the final product (i.e. the PM_{10} concentration maps) the whole uncertainty associated with the unknowns (data, parameters, model structure). A practical air quality management strategy must inform decision makers and stakeholders of such uncertainties, in a straightforward and direct manner (Liu et al., 2008).

Bayesian hierarchical models (Clark & Gelfand, 2006) are another common approach in air quality studies (Blangiardo et al., 2019; Huang et al., 2018; Shaddick et al., 2017; Forlani et al., 2020). This approach allows to model complex phenomena as a hierarchy of simpler sub-models, making it possible to deal with the complexity of spatio-temporal processes in a straightforward way. Covariates as orography or temperature can be used to explain the large scale variability of the phenomenon under study, while residual dependency can be modelled through a space-time process which is usually assumed to be a Gaussian Random Field (GRF). Moreover, the Bayesian approach allows to easily take into account the variability related to models and parameters, thus giving a more realistic picture of the uncertainty of the final estimates.

The main drawback is that GRF is hard to deal with when there is a lot of data, making its use for environmental applications on large scale challenging (Porcu et al., 2012). Most of the studies using hierarchical models with spatial GRF concern relatively small areas such as cities (Pollice & Jona Lasinio, 2010; Sahu, 2011) or regions (in the Italian context see for example Cameletti et al., 2011; Cocchi et al., 2007; Grisotto et al., 2016) or consider large domains but without the temporal component (Beloconi et al., 2018). In addition, the main inferential tool for Bayesian hierarchical models, namely the Markov chain Monte Carlo (MCMC) approach (Gilks et al., 1995), despite the existence of user friendly programming tools like `WinBUGS` (Spiegelhalter et al., 1995), `JAGS` (Plummer, 2016) and `Stan` (Team, 2015), can be viewed by the applied community as rather cumbersome, requiring a lot of CPU-time as well as tweaking of simulation and model parameters' specifications.

Some strategies have been proposed to alleviate the computational burden of fitting complex spatio-temporal hierarchical models (Heaton et al. (2019) for an updated review). One of such strategies, the so-called SPDE (Stochastic Partial Differential Equation) approach, has received a lot of attention in recent years (see Bakka et al., 2018 and reference therein). The SPDE approach provides a way to represent a continuous GRF through a discretely indexed Gaussian Markov Random Field (GMRF; Lindgren et al., 2011). Computationally, GMRFs are much more efficient as they are based on sparse matrices (Rue & Held, 2005). Moreover, GRF with a SPDE representation can be fitted in a Bayesian hierarchical framework using the Integrated Nested Laplace approximation (INLA) approach (Rue et al., 2009). INLA is a deterministic method based on approximating the marginal posterior distributions (by using Laplace and other numerical approximations and numerical integration schemes) and is usually faster and more accurate than MCMC alternatives. Last, but not least, INLA-SPDE comes with a user friendly `R` implementation, the `r-inla` package. Tutorials and examples are available at the dedicated web site `r-inla.org` or in book form (e.g. Blangiardo & Cameletti, 2015; Gòmez-Rubio, 2020). This makes the INLA-SPDE methodology a fast, reliable and easy to use tool also to the practitioners.

In this paper we tested the INLA-SPDE approach to estimate PM_{10} daily concentrations on a large space-time domain, namely the entire Italian territory (18 conterminous regions plus two major islands), for one year (2015) based on ground daily PM_{10} records on ca 400 stations. The final result is a collection of high resolution (1 Km $\times$ 1 Km) daily maps of PM_{10} concentrations with an associated measure of uncertainty. Such maps can aid responsible authorities and decision-makers for the development of risk assessment and environmental policies.

The rest of the paper is organized as follows: in Section 2 we present the input dataset and introduce the statistical model we have chosen to analyse the PM_{10} concentrations. Section 3 discusses results, model validation and two possible applications of the model estimates for the assessment of air quality in

Italy. We end with conclusions in Section 4.

2. Material and Methods

2.1. Spatial domain

The Italian peninsula extends into the Mediterranean sea with a narrow and long shape of about 7500 km of coast line. It includes two large mountain systems (the Alps to the north, and the Apennines which extend north-west to south along the country), a large plain (the Po Valley with a surface of 46000 km^2) and two major islands (Sicily and Sardinia). This complex orography leads to a variety of climatic conditions which exert a strong influence on the observed spatial and seasonal variability of pollutants concentrations (Perrino et al., 2020).

Because of its central position in the Mediterranean Basin, Italy is also affected by periodic Saharan dust events which influence air quality. Multiple studies (Matassoni et al., 2009; Pey et al., 2013; Barnaba et al., 2017; Pikridas et al., 2018) have estimated the impact of such events on the yearly average PM_{10} values in the range 1 - 9 $\mu g/m^3$, with concentrations decreasing towards the north. There is evidence that this increase in PM_{10} levels has a further negative impact on human health (Tobías et al., 2011).

2.2. Monitoring sites and concentrations data

This study is based on the 2015 PM_{10} daily average concentrations ($\mu g/m^3$) belonging to the Regional Environmental Agencies (ARPA) and collected by the Italian Institute for Environmental Protection and Research (ISPRA). PM_{10} mass concentrations were determined using the European reference or equivalent methods. The data were fully validated accordingly to standard QA/QC procedures Directive 2008/50/EC (EU, 2008). The data set originally accounted for more than 500 monitoring sites. To work with a more robust dataset, we have kept only stations that had at least 10 valid daily mean concentrations for each month. The geographical distribution of the final 410 selected stations is shown in Figure 1. Note that a large portion of the selected time series (83%) are characterized by low data missingness, having at least 20 valid daily mean concentrations per month.

The ground PM_{10} monitoring stations are mostly located in urban and suburban areas (244 urban stations, 104 suburban and 62 rural). Low elevations are over represented with 75% of the monitoring sites lying below 250 m. This bias is not unexpected, as high-level polluted areas typically require denser networks (EU, 2002).

The boxplot of Figure 2 shows the PM_{10} monthly distribution. During 2015, PM_{10} daily concentrations ranged between 0 and 337 $\mu g/m^3$, with a median daily PM_{10} concentrations of 22.3 $\mu g/m^3$ and an inter-quartile range of 15 and 33 $\mu g/m^3$. The boxplots suggest a seasonal trend in the observational data: higher PM_{10} levels, with an average daily median around 30 $\mu g/m^3$, characterize the beginning (January-March) and the end (November-December) of 2015. Conversely, lower values were recorded during spring and summer seasons when the average daily median is around 19 $\mu g/m^3$. A similar trend characterizes the standard deviation with values around 24 $\mu g/m^3$ during the winter months (January-February-December), 14 $\mu g/m^3$ during the intermediate seasons (March-April-September-October-November) and 9 $\mu g/m^3$ in summer including May.

To conclude this section, we observe that, except for April, all months exhibit occasionally daily values greater than 100 $\mu g/m^3$. The three highest values in our input dataset were observed in January (211 $\mu g/m^3$), in August (196 $\mu g/m^3$) and in December (337 $\mu g/m^3$). Despite the outlier nature of these values, the full PM_{10} distribution was considered and no value was discarded from our analysis.

2.3. Predictors

A large number of potential predictors were available. Based on previous results in the air quality literature and a preliminary analysis of our data, a set of eleven spatial and spatio-temporal predictors was selected to be included in

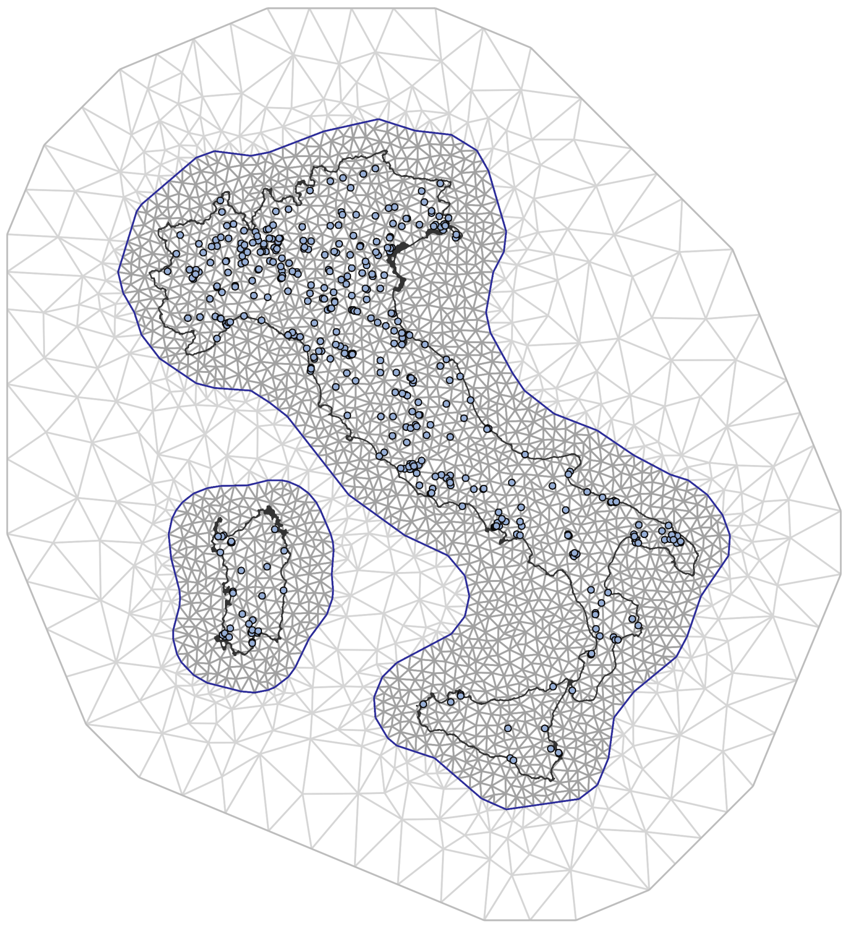

Figure 1: Study domain together with the spatial distribution of the 410 monitoring sites. The Figure illustrates also the mesh used to build the SPDE approximation to the continuous Matérn field.

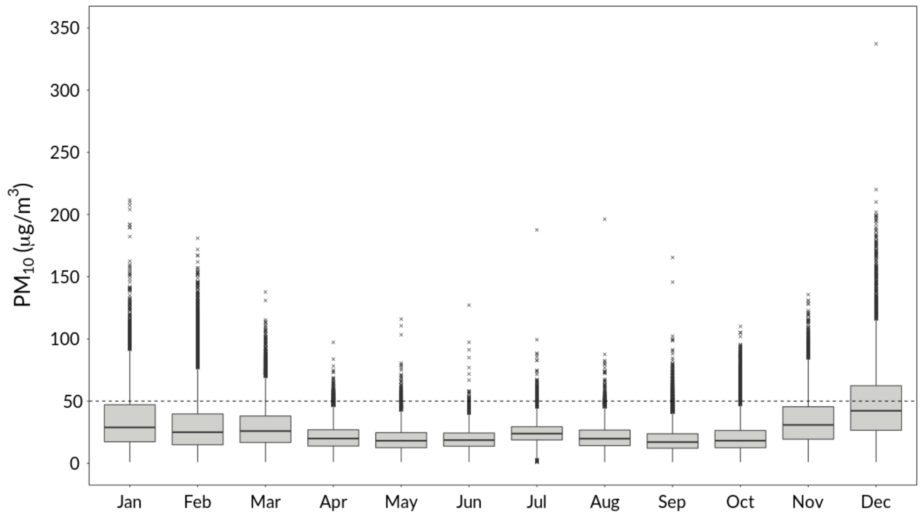

Figure 2: Monthly distribution of the daily PM_{10} concentrations for year 2015. The dashed line indicates the European Community PM_{10} daily limit value not to be exceeded more than 35 days a year.

the model by using variable selection methods. The complete list is reported in Table 1.

To avoid numerical problems, each predictor (except for the dust indicator) was standardized to have mean 0 and standard deviation 1.

In the following, we describe the selected predictors more in details.

Meteorological variables. Pollutant concentrations are highly dependent on weather conditions (Grange et al., 2018), therefore metereological variables are an important part of our model. Hourly surface pressure, total precipitation and temperature at 2 meters height were downloaded as netCDF archives from the ERA5 reanalysis dataset (Hersbach et al., 2020) of the European Centre for Medium-Range Weather Forecasts (ECMWF). Hourly data were averaged (accumulated, in the case of precipitation) on a daily level. As particulate matter levels depend also on the recent weather history, we have also introduced the variable "total precipitation of the previous day" (Barmpadimos et al., 2012). Planet Boundary Layer height (PBL) is the height up to which the influence of

Data Source	Variable Code	Description	Unit	Spatial Resolution
ERA5				
	pbl00	Planet Boundary Layer at 00:00	m	31 Km
	pbl12	Planet Boundary Layer at 12:00	m	
	ptp	Previous day Total Precipitation	mm	
	sp	Surface Pressure	hPa	
	t2m	Average temperature at 2 meters	°C	
	tp	Total Precipitation	mm	
Copernicus Atmosphere Monitoring Service				
	aod550	Aerosol Optical Depth at 550 nm	nm	~10 Km
Global Multi-resolution Terrain Elevation Data				
	q_dem	Altitude	m	1 Km
NMMB-BSC; HYSPLIT-NOAA				
	dust	Saharan dust	0/1	Macroareas
OpenStreetMap				
	d_a1	Linear distance to the nearest highway	m	1 km
Copernicus Land Monitoring Service				
	i_surface	Imperviousness	%	100 m

Table 1: List of the predictors included in the spatio-temporal model.

the presence of the lower surface is detectable (Shi et al., 2020). PBL at 00:00 and 12:00 was also obtained from the ERA5 dataset and log transformed.

Aerosol Optical Depth. Aerosol Optical Depth is a key parameter to measure the aerosol "column burden" (Hidy et al., 2009). Namely, it represents the extinction of the solar radiation in the atmospheric column attributed to aerosols (Segura et al., 2017). PM_{10} has been shown to correlate with Aerosol Optical Depth (Di et al., 2016). In this study, we used numerically simulated estimates of AOD data at the wavelength of 550 nm from the CAMS reanalysis (Copernicus Atmosphere Monitoring Service), whose horizontal spatial resolution is of about 10 kms. The interesting aspect of such data is that it does not suffer from the presence of non-random missing values, which typically affect the well-known satellite product AOD from the Multi-Angle Implementation of Atmospheric Correction (MAIAC) algorithm (Lyapustin et al., 2018).

Elevation. Elevation data were retrieved from the Global Multi-resolution Terrain Elevation Data of the USGS (Danielson & Gesch, 2011) at a 30-arc-second (ca 1Km $\times$ 1Km) resolution.

Dust events. In our model, the occurance of dust events is described in terms of a dichotomic variable (dust event/no-dust event). The days with dust events have been identified using simulation models (NMMB/BSC-Dust model; Pérez et al., 2011) and Lagrangian models for the simulation of trajectories (HYSPLIT; Stein et al., 2015). The final information is available for 5 Italian macro-areas: North, Centre, South, Sicily and Sardinia.

Road traffic emissions. Different proxy variables were considered to estimate the impact of road traffic emissions, but only the Euclidean distance from the major roads (highways) entered the final model. The road network data come from the OpenStreetMap project (Haklay et al., 2010) and were downloaded as .pbf (vector) files from the Geofabrik web service (`www.geofabrik.de`).

Impervious surface. Imperviousness represents the percentage of soil sealing (the covering of land by an impermeable material). Imperviousness is a key indicator of urbanization which provides an estimation of population distribution (Attarchi, 2020). The degree of imperviousness (0-100%) was downloaded as a GeoTIFF raster file from the Copernicus Land Monitoring Service (Langanke, 2018).

2.4. Statistical Modeling

Let $y^m(t, s_i)$ denote the realization of the space-time process $Y^m(t, s_i)$ that represents the log PM_{10} concentrations at day $t = 1, \ldots, T^m$ of month $m = 1, \ldots, 12$ at location s_i, $i = 1, \ldots, 410$. The logarithmic transformation is a typical choice for data with highly right skewed distributions (Ott, 1990; Warsono et al., 2001) like the PM_{10} data reported in Figure 2.

Our exploratory analysis (results not shown for sake of brevity) highlighted that the impact of each predictor on PM_{10} concentrations varies across time. Consequently, we developed twelve models, one for each month of the year, all containing the same terms. A similar approach is documented, for example, in Al-Hamdan et al. (2009) for the estimation of $PM_{2.5}$ concentrations in the Atlanta metropolitan area using AOD data.

We assumed the following model:

$$y(t, s_i) = \mu + \mathbf{x}(t, s_i)\boldsymbol{\beta}' + u(t, s_i) + z(s_i) + \epsilon(t, s_i) \tag{1}$$

Since the models are identical for each month, in the above formula we have omitted the index m to simplify the notation. In Equation (1), μ is the intercept, $\mathbf{x}(t, s_i) = \big(x_1(t, s_i), \ldots, x_p(t, s_i)\big)$ denotes the vector of predictors at site s_i in day t (see Table 1) and $\boldsymbol{\beta} = \big(\beta_1, \ldots, \beta_p\big)$ is the corresponding coefficients vector. The term $\epsilon(t, s_i)$ represents measurement error and is defined by a Gaussian white noise process independent over space and time with standard deviation σ_ϵ. The process $u(t, s_i)$ represents the residual space-time correlation once the large scale component $\mathbf{x}(t, s_i)\boldsymbol{\beta}'$ is taken into account. As particulate levels are characterized by inter-daily correlation, we assumed $u(t, s_i)$ to change in time according to a first order autoregressive process with spatially colored innovations:

$$u(t, s_i) = a\ u(t-1, s_i) + \omega(t, s_i)$$

for $t = 2; \ldots, T-1$, $|a| < 1$. We assumed the innovation $\omega(t, s_i)$ to be a Gaussian process with mean 0 and covariance function given by:

$$\mathrm{Cov}(\omega(t, s_i), \omega(t', s_j)) = \begin{cases} 0, & \text{for } t \neq t' \\ C(h), & \text{for } t = t' \end{cases} \tag{2}$$

where $h = ||s_i - s_j||$ is the Euclidean distance between sites i and j. A common specification for the purely spatial covariance function $C(h)$ is the Matérn function:

$$C(h) = \sigma_\omega^2 \frac{1}{\Gamma(\nu) 2^{\nu-1}} (k\ h)^\nu K_\nu(k\ h)$$

where σ_ω^2 is the marginal variance of the process and $K_\nu(\cdot)$ denotes the Bessel function of second kind and order $\nu > 0$. The parameter ν measures the degree of spatial smoothness of the process. This parameter is hard to estimate and is usually fixed to a given value rather than estimated, with $\nu = 1$ a common choice (Blangiardo & Cameletti, 2015). The term $k > 0$ is a scaling parameter related to the range ρ, i.e. the distance at which the spatial correlation becomes small. Following Lindgren et al. (2011), we used the empirically derived definition $\rho = \frac{\sqrt{8\nu}}{k}$, with ρ corresponding to the distance where the spatial correlation is close to 0.1, for each ν. To represent the continuous field $u(t, s_i)$ as a GMRF, we used the SPDE approach (Lindgren et al., 2011), which is based on the finite element method (fem). The triangulation used for fem in our case is shown in Figure 1. In order to obtain accurate approximations of the underlying GRF, the triangular mesh must be dense enough to capture the spatial variability of daily PM_{10}. It is noteworthy to observe that we constructed a mesh which is rather dense over areas with observations and sparser in the outer region, where no data are observed and where we are not interested in prediction. The purpose of the outer mesh is to avoid boundary effects and its sparse triangulation allows to reduce computational costs.

Finally, the last term in Equation (1) is defined as $z(s_i) \sim N(0, \sigma_z^2)$ and is a spatially uncorrelated Gaussian random effect which captures some of the small scale spatial variability.

2.5. Priors definition

In a Bayesian context, in order to finalize the model we need to define prior distributions for the vector $\boldsymbol{\beta}$, the standard deviations $\sigma_\epsilon, \sigma_z$, σ_ω, the autocorrelation parameter a in Equation (2) and the range ρ of the Matérn function. We used vague Gaussian priors for the elements of $\boldsymbol{\beta}$ and Penalized Complexity (PC) priors (Simpson et al., 2017) for the other parameters. The latter are designed to penalize model complexity and avoid overfitting. PC priors for the standard deviation parameters can be defined through $\text{Prob}(\sigma > u_\sigma) = \alpha_\sigma$ where $u_\sigma > 0$ is a quantile of the prior and $0 \leq \alpha_\sigma \leq 1$ is a probability value. In our study we set $u_\sigma = 1$ and $\alpha_\sigma = 0.01$ for both $\sigma_\epsilon, \sigma_z$. The choice was motivated by the fact that the total standard deviation of the observed log PM_{10} values varies between 0.4 and 0.8 depending on the month, therefore it is very likely for the variance of each component to be less than 1. For ρ and σ_ω we used the joint PC prior suggested in Fuglstad et al. (2019) which can be specified through

$$\text{Prob}(\rho < u_\rho) = \alpha_\rho;\ \text{Prob}(\sigma_\omega > u_{\sigma_\omega}) = \alpha_{\sigma_\omega},$$

where we set $u_\rho = 150$, $\alpha_\rho = 0.8$, $u_{\sigma_\omega} = 1$, $\alpha_{\sigma_\omega} = 0.01$. Since the large scale spatial dependence is explained by the covariates, it is reasonable to assume the range of the innovation process to be smaller than 150 Km. Finally, for the autocorrelation parameter a we used the PC prior proposed in Sørbye & Rue (2017). This can be specified through $\text{Prob}(a > u_a) = \alpha_a$, where we set $u_a = 0.8$ and $\alpha_a = 0.4$. The choice was guided by previous findings (e.g. Cameletti et al., 2013) and restrictions to the possible values of u_a and α_a.

2.6. Implementation

All data processing was performed through the combined use of the Climate Data Operator (`CDO`) software (`https://code.mpimet.mpg.de/projects/cdo`), the `R` statistical language (R Core Team, 2018) and `PostGIS` (Strobl, 2008).

Data analysis and modeling have been performed using the `r-inla` package. Input data and excerpts of the `R` code for the definition of the PC priors and the model fit are available at `https://github.com/guidofioravanti/spde_spatio_temporal_pm10_modelling_italy`.

3. Results and discussion

In this section we first discuss parameter estimates and residual analysis for the 12 monthly models. We then show a cross-validation study aimed at assessing the model performance. Finally, we present some additional outcomes based on the PM_{10} spatial predictors available for the 1Km $\times$ 1Km grid covering the whole Italian territory.

3.1. Parameter estimates

Figure 3 illustrates the posterior distribution for the model intercept μ and the 11 covariate coefficients $\boldsymbol{\beta}$ for each of the 12 monthly models.

As expected, many of the parameters show a clear seasonal behaviour. The posterior mean of μ varies from a minimum of 2.42 in July to a maximum of 3.4 in December on the log scale. This corresponds to an average pollution level that varies between 11.2 and 40.0 $\mu g/m^3$, after adjustment for covariates.

The predictors with the most pronounced seasonal effect are: temperature (t2m), Planet Boundary Layer at 00:00 (pbl00), altitude (q_dem) and impervious surface (i_surface). Temperature tends to have a positive effect during the summer months and a negative or null effect during the winter months; pbl00 and altitude have negative effects on the log PM_{10} concentrations, with a stronger magnitude in the winter season. Conversely, the impervious surface has a positive effect, which also tends to be larger in winter.

In general, all the covariates, including AOD, have a stronger effect in winter time, when the PM_{10} levels are higher and more variable both in space and time. Interestingly, we point out that a seasonal effect of the AOD has been reported

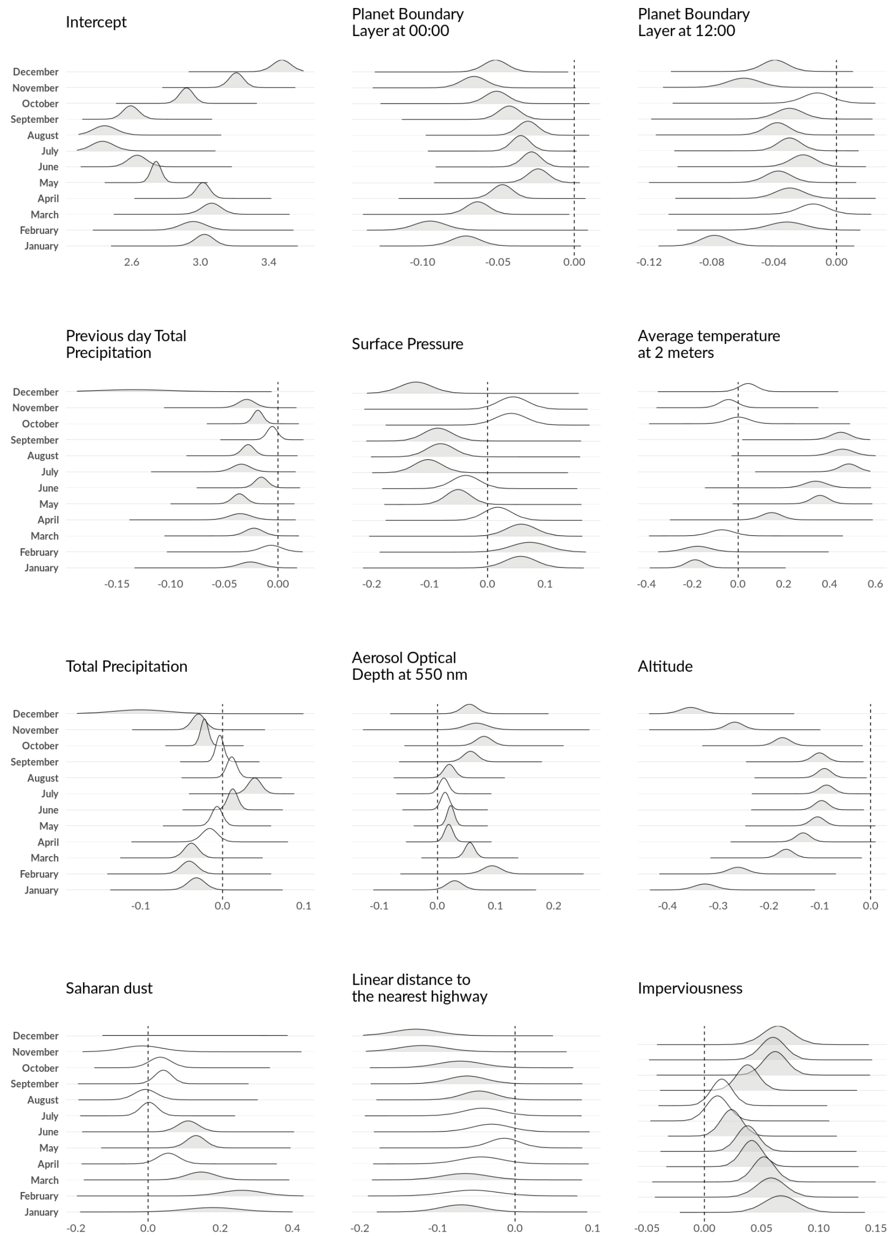

Figure 3: Tmax: posterior distribution of the intercept $\boldsymbol{\mu}$ and covariate coefficients $\boldsymbol{\beta}$. The shaded color indicates a statistically significant effect.

also in Al-Hamdan et al. (2009), but of opposite sign (weaker during the cool season and relatively strong during the warm season).

The seasonal-varying effects shown in Figure 3 support our initial hypothesis that a monthly regression analysis could improve the accuracy of the final estimates (Weber et al., 2010).

The posterior standard deviation (sd) of the $\boldsymbol{\beta}$ parameters (which can be inferred from the shape of the posterior distributions in Figure 3) is rather stable from month to month. Exceptions are the sd for the distribution of the dust indicator and the total precipitation (same and previous day) in December. These standard deviations are much larger that those in the other months, as a result of no-occurrence of dust events and localized and scarce precipitation events in December 2015.

Estimates of the other model parameters (posterior means and standard deviations) are reported in Table 2. We observe that the spatial component shows higher variability than both the measurement error and the spatial unstructured effect. All the three standard deviations have a seasonal variation, being higher in winter than in summer. The spatial range parameter ρ also presents a variation across months. The posterior mean goes from a minimum of ca 106 Km in January to a maximum of ca 239 Km in August. There is a clear tendency for the spatial range of the Gaussian process $u(t, s)$ to be larger in summer, corresponding to a spatially smoother particulate matter field; the same behaviour holds for the posterior standard deviation of the same model component. This result reflects the fact that, in summer time, the PM10 concentrations are characterized by low spatial variability mostly explained by the model predictors.

Finally, the posterior mean of the AR(1) autocorrelation coefficient a oscillates from 0.62 to 0.82 but there is no clear seasonal pattern. The rather high value of the autocorrelation coefficient confirms the presence of short-term persistence of the PM_{10}.

In order to assess whether the model manages to capture the spatio-temporal variability of the PM_{10} observations, we show in Figure 4 the spatio-temporal

	a	ρ	σ_z	σ_ϵ	σ_ω
January	0.629 (0.018)	106.23 (4.186)	0.247 (0.012)	0.197 (0.002)	0.434 (0.011)
February	0.656 (0.017)	135.213 (5.341)	0.207 (0.01)	0.201 (0.002)	0.513 (0.014)
March	0.656 (0.018)	192.579 (8.498)	0.162 (0.008)	0.18 (0.002)	0.432 (0.014)
April	0.742 (0.019)	153.914 (8.29)	0.151 (0.007)	0.178 (0.002)	0.361 (0.014)
May	0.624 (0.02)	167.292 (9.017)	0.163 (0.007)	0.177 (0.002)	0.289 (0.008)
June	0.743 (0.023)	237.997 (15.118)	0.157 (0.006)	0.167 (0.001)	0.282 (0.013)
July	0.823 (0.018)	177.433 (10.544)	0.163 (0.007)	0.155 (0.001)	0.263 (0.014)
August	0.704 (0.022)	238.714 (15.483)	0.159 (0.006)	0.177 (0.001)	0.256 (0.011)
September	0.697 (0.019)	181.108 (9.8)	0.161 (0.007)	0.177 (0.002)	0.319 (0.011)
October	0.727 (0.017)	164.188 (7.097)	0.171 (0.007)	0.176 (0.002)	0.382 (0.013)
November	0.78 (0.014)	105.514 (3.908)	0.167 (0.009)	0.153 (0.002)	0.443 (0.014)
December	0.825 (0.014)	83.96 (2.968)	0.209 (0.012)	0.148 (0.002)	0.41 (0.015)

Table 2: Posterior means (standard deviations) of the parameters in all 12 models.

variograms (Cressie & Wikle, 2011) for the log PM_{10} concentrations (solid lines) and for the model residuals (dotted lines).

For the log PM_{10} concentrations the semi-variance increases with distance (x-axis), suggesting spatial dependence among observations. A similar behaviour is apparent when we look at the semi-variance along the y-axis (time), having fixed a distance on the x-axis: in this case, the semi-variance increases with the time-lag, reflecting temporal dependence in the data. None of these patterns can be seen in the corresponding residuals variograms, indicating that the models capture the spatio-temporal signal and return uncorrelated residuals.

3.2. Validation

To evaluate the predictive performance of the model we did a cross-validation study similar to the one presented in Pirani et al. (2014). Specifically, we stratified the 410 input monitoring sites into three groups according to their area type category (urban, suburban and rural). A validation dataset was identified by sampling 10% of the monitoring sites in each group (24 urban sites, 11 suburban and 6 rural), with the rest of the stations labelled as training dataset. We used the training dataset to fit the model and predict PM_{10} concentrations on the

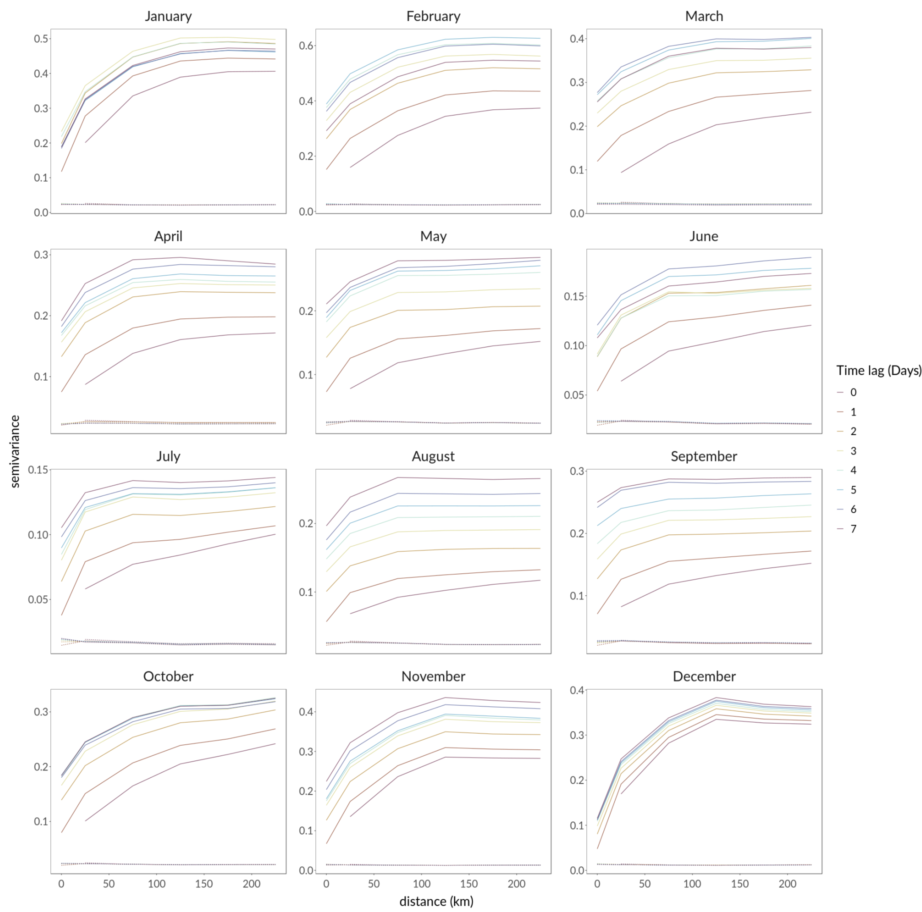

Figure 4: Monthly spatio-temporal variograms for the observed (log) PM_{10} concentrations (solid lines) and the corresponding model residuals (dashed lines).

validation dataset. Finally, we compared the predicted values to the observed ones and summarised the results using a series of performance measures. The sampling process was repeated three times (trials), resulting in three validation and training datasets.

As performance measures we chose the following indices: 1) the empirical coverage of 95% credible intervals (95% CI); 2) the correlation coefficient; 3) the root mean square error (RMSE); 4) the bias. The last three indexes are computed by comparing the observed concentrations and the posterior predicted means of each monitoring site. For each training/validation dataset, the average of each performance score over all stations was computed. Table 3 reports the global model performance in terms of average scores over the three different trials. All indices are on the original scale for ease of communication to the practitioners and the end users.

Generally speaking, it appears that the models perform well both in the training and in the validation phase. RMSE values are higher in the winter months for both phases. This is not surprising since in winter we observe higher particulate concentrations.

The high values of the correlation coefficients (above 0.9 for all months in the training phase and and above 0.7 in the validation phase) show that the predicted and the observed values are well in accordance. This can be also seen from Figure 5 where we have plotted the predicted versus the observed values. To avoid having too many scatterplots, in Figure 5 we adopted a seasonal representation.

The plots highlight that the points are distributed uniformly along the diagonal line. However, a general underestimation of high concentrations values is apparent in all seasons both in the training and validation stage. In particular, we see that the model fails to reproduce very high concentrations above 150 $\mu g/m^3$.

Back to Table 3, a negligible bias can be observed, with absolute values less than 1.1 $\mu g/m^3$ in all months. Finally, the empirical coverage is very close to its nominal value of 95%.

	RMSE $\mu g/m^3$		**Correlation**		**Bias** $\mu g/m^3$		**Coverage** %	
	Training	*Validation*	Training	*Validation*	Training	*Validation*	Training	*Validation*
January	5.33	*11.14*	0.98	*0.87*	-0.04	*1.07*	98.23	*94.93*
February	4.87	*9.59*	0.98	*0.91*	-0.1	*0.62*	98.10	*94.41*
March	4.24	*7.43*	0.97	*0.89*	-0.07	*0.54*	97.66	*94.64*
April	3.08	*5.60*	0.95	*0.83*	-0.03	*0.49*	97.61	*93.74*
May	3.06	*5.31*	0.95	*0.83*	-0.03	*0.28*	97.86	*95.16*
June	3.02	*4.84*	0.93	*0.79*	-0.02	*0.25*	97.31	*94.43*
July	3.47	*6.38*	0.92	*0.71*	-0.01	*0.29*	97.41	*94.56*
August	3.68	*5.41*	0.92	*0.82*	-0.03	*0.22*	97.05	*95.62*
September	3.68	*5.63*	0.94	*0.85*	0.01	*0.55*	97.51	*95.24*
October	3.21	*6.05*	0.97	*0.89*	-0.01	*0.61*	97.80	*94.61*
November	3.77	*8.92*	0.98	*0.88*	-0.01	*0.73*	98.44	*93.57*
December	5.79	*13.90*	0.98	*0.83*	0.04	*0.79*	98.53	*95.48*

Table 3: Statistics of the cross-validation study (on original scale).

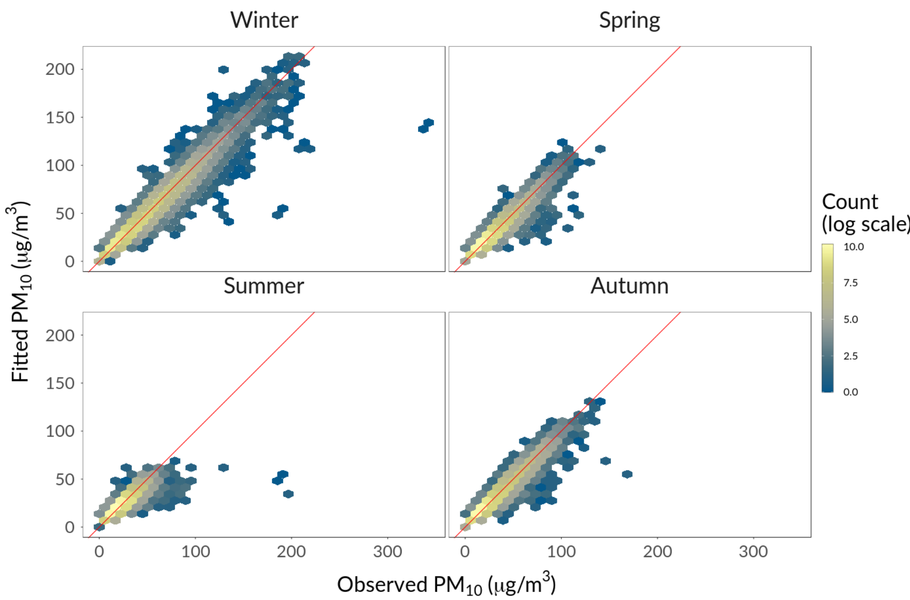

(a) Training Stage

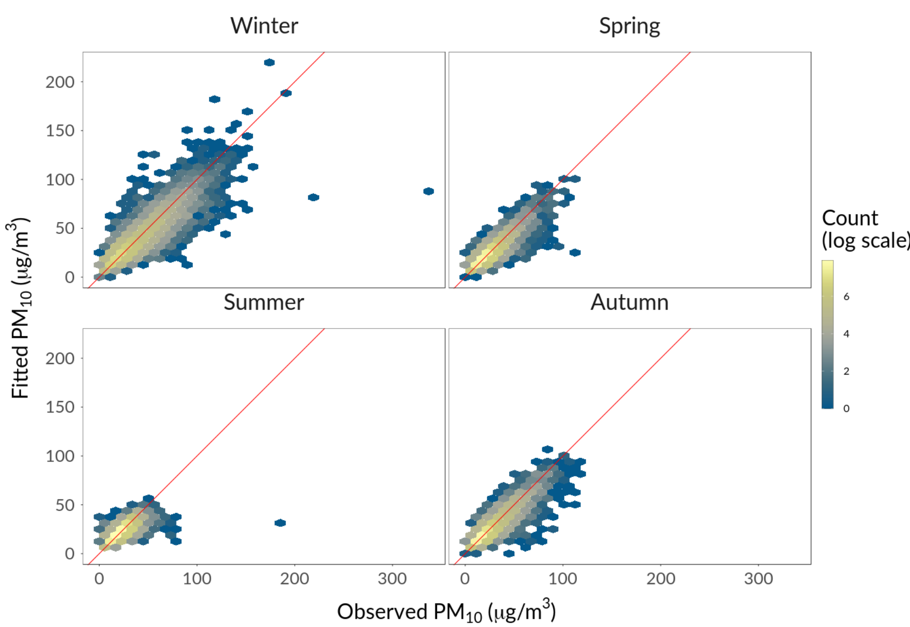

(b) Validation Stage

Figure 5: Agreement between modelled and measured PM_{10} concentrations. Lighter colors indicate areas with higher points concentrations. The solid line is the 1:1 line as a reference.

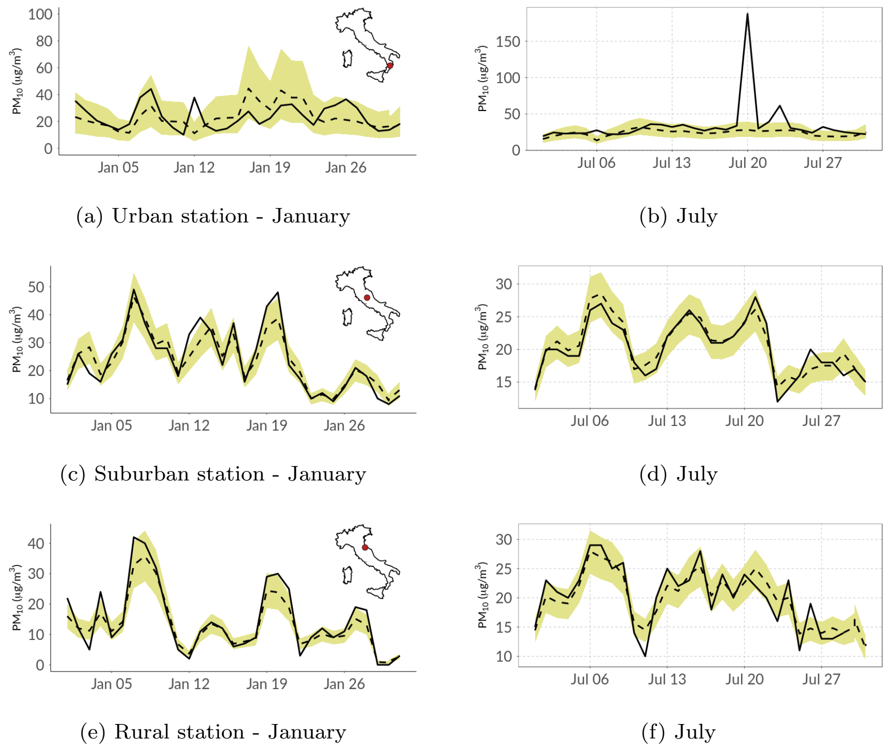

(a) Urban station - January

(b) July

(c) Suburban station - January

(d) July

(e) Rural station - January

(f) July

Figure 6: PM_{10} daily concentrations for three illustrative monitoring sites, one for each type area category: urban (Santa Maria station), suburban (Santo Chiodo station) and rural (San Leo station). Observed (solid lines) versus fitted values (dashed lines).

Figure 6 shows a comparison between observed and predicted time series for 3 illustrative stations chosen from the validation set. For sake of brevity, we present the results for two months alone: January and July. The time series plots suggest that the model is able to reproduce the temporal variability of the monitoring sites in the validation dataset, although some very high values (for example in the upper right panel of Figure 6) are not properly captured.

3.3. Spatial Prediction

In this section, we focus on spatial predictions. In particular, we provide examples of daily and monthly maps, using a 1km × 1km grid over the whole Italian territory. This results in a spatial grid of 310622 cells which, across the entire year 2015, corresponds to a spatio-temporal grid of over 11 millions cells.

We have simulated 1000 samples from the posterior distribution of all model components for two months. We chose January and July 2015 in order to show some of the seasonal characteristics of the fitted model. Having a sample distribution of 1000 gridded maps for each day of January and July 2015, we were able to calculate summary statistics of central tendency (mean) and variability (sd).

As an example, Figure 7 a) and b) show the posterior mean of the daily PM_{10} concentrations on January 26th and July 21st 2015. These two dates were chosen randomly and have no special meaning. Note that the two figures have different color scales. A visual inspection of Figure 7 a) and b) highlights that the interpolation procedure is able to reproduce the large-scale data features without unrealistic artifacts in the generated surfaces. Specifically, both daily maps exhibit a reasonable spatial pattern of high PM_{10} mean concentrations in urbanized environments, which decrease in rural areas and with altitude. This is especially apparent in the January map, when the model estimates high PM_{10} levels in the Po Valley with a peak above 50 $\mu g/m^3$ in the Turin city area (North-Western Italy). In July, the model generates a smoother surface with less spatial variability. The orography here, for example, is visible but less pronounced than in January. This result is not unanticipated: it reflects the results seen in Table 2, the greater range and lower variability of the latent spatial field in summer with respect to the winter time. These results, in turn, depend on the seasonality of the PM_{10} concentrations illustrated through the boxplots of Figure 2.

A video, describing the entire temporal evolution of the daily PM_{10} concentrations for both months of January and July 2015 is available at `https://github.com/guidofioravanti/spde_spatio_temporal_pm10_modelling_italy`.

We use the relative width of the posterior interquartile range (RWPIR) as a measure for the relative uncertainty of the predicted concentrations surface (Yuan et al., 2017):

$$RWPIR = (Q_3 - Q_1)/Q_2,$$

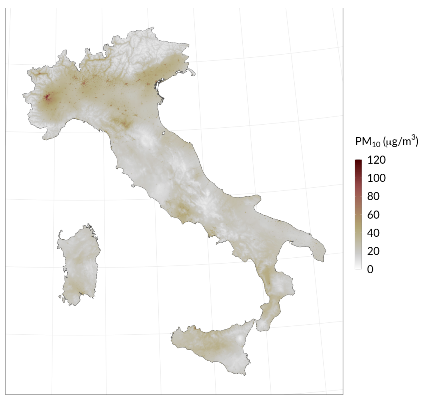

(a) January 26th

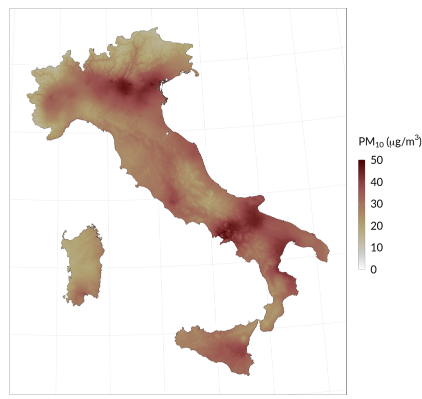

(b) July 21st

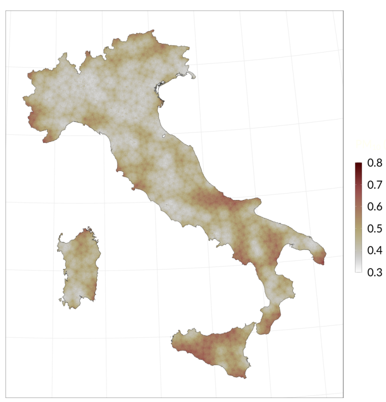

(c) January 26th

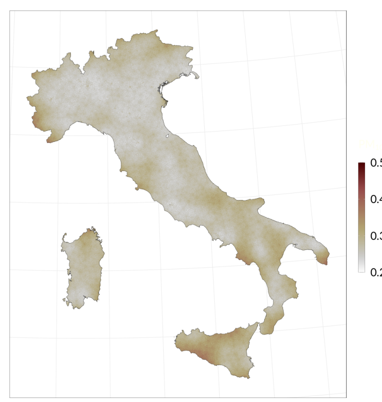

(d) July 21st

Figure 7: Posterior daily mean PM$_{10}$ concentrations maps (a-b) and relative width of the posterior interquartile range (c-d) for January 26th and July 21st, 2015.

where Q_1, Q_2 and Q_3 are the first quartile, the median and the third quartile.

The RWPIR for the two selected days is shown in Figure 7 c) and d) for January 26th and June 21st, respectively. As expected, the relative uncertainty is higher in January than in July but the spatial pattern in Figure 7 c) and d) is quite similar: uncertainty is lower where there are more monitoring sites and higher otherwise.

Analogous considerations apply when we examine the monthly average concentrations maps. Figure 8 a) and b) show the posterior monthly PM_{10} average concentrations while Figure 8 c) and d) shows the RWPIR. In this case, the simulated daily prediction surfaces were aggregated in order to create a corresponding sample of 1000 average monthly concentrations maps.

3.4. Model applications

This section shows two potential applications of our model estimates for the assessment of air quality in Italy: population exposure to PM_{10} and exceedance probability maps.

Population exposure to PM_{10}. The goal of many air pollution epidemiology studies is to estimate the effect of air pollution on health (Sheppard et al., 2005). In this sense, comparing a limit value with the modeled concentrations is not sufficient for public health purposes, as it does no make any assumption about human exposition (the event of contact with a pollutant over a certain period of time) to air pollution (Zou et al., 2009).

Here, we combine the population density data and the model output concentrations to estimate the population exposure to PM_{10} pollution in Italy at the municipality level.

For the targeted municipality m, the population-weighted PM_{10} concentration level e^m is given by:

$$e^m = \frac{\sum_{i \in I_m} p_i \ c_i}{\sum_{i \in I_m} p_i} \tag{3}$$

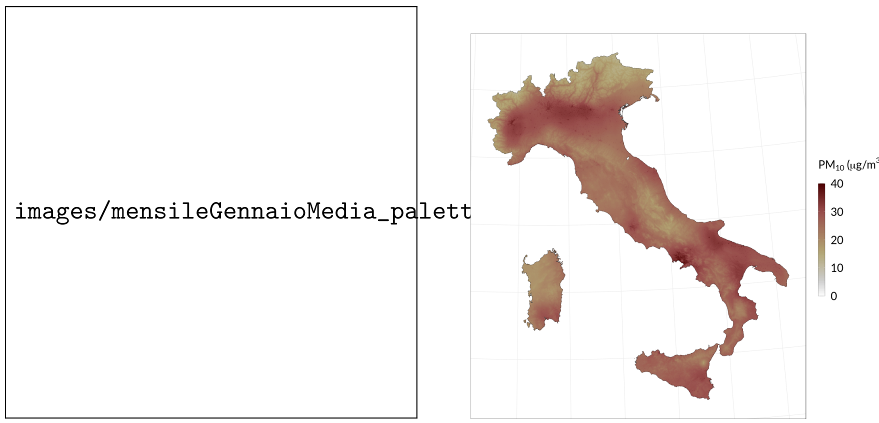

(a) January (b) July

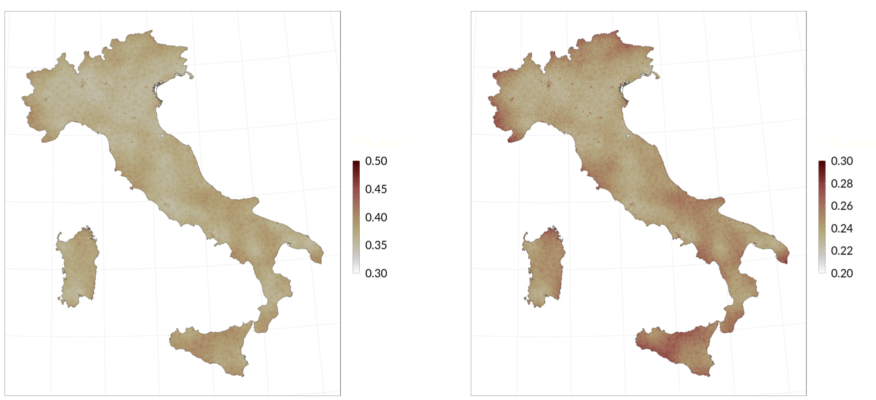

(c) January (d) July

Figure 8: Monthly average PM_{10} concentrations maps (a-b) and relative width of the posterior interquartile range (c-d) for January and July 2015.

where I_m is the set of of grid cells within the administrative unit m; p_i and c_i denote the population density and PM_{10} concentration level in the i^{th} grid cell of m, respectively.

For the considered case study, the PM_{10} concentration levels c_i are (a) the PM_{10} annual mean concentrations, (b) the annual 90.4 percentile and (c) the annual 99.2 percentile, calculated using the 365 daily interpolated surfaces discussed in Section 3.3. For the population density data, we used the national grid (1km × 1km) of the population density for 2011 of the Italian National Institute of Statistics (ISTAT, `https://www.istat.it/it/archivio/155162`). The final maps are displayed in Figure 9.

The maps highlight the particular vulnerability to exposure to particulate pollution of the Po Basin, as well as the existence of other areas (the Sacco Valley and the Terni Basin in Central Italy, the agglomeration of Naples and Caserta in the south) where people are exposed to average levels above the WHO guidelines (20 $\mu g/m^3$ for the annual average) and the annual limit value settled by the European legislation (40 $\mu g/m^3$). The percentile maps (Figure 9 b and c) indicate respectively the areas where the EU air quality limit value for PM_{10} daily concentrations is exceeded (i.e., areas where the 90.4 percentile is higher than 50 $\mu g/m^3$), and the areas where the more severe WHO air quality guideline for short-term exposure (24-hours) is exceeded (99.2 annual percentile higher than 50 $\mu g/m^3$). The widespread exceedances of the air quality guidelines over the Italian territory arise the need to adopt more stringent policies to further reduce the anthropogenic emissions of PM and those of their precursors.

Exceedence. To assess the risk of a pollutant, monitoring stations can be classified in terms of probabilities of exceeding (POE) a certain limit value (Denby et al., 2011). For example, Yang et al. (2016) show maps of probabilities of $PM_{2.5}$ concentrations exceeding 25 $\mu g/m^3$ for the Shandong Province (China). Similarly, in Blangiardo et al. (2013) and Blangiardo & Cameletti (2015) the map of the posterior probability of exceeding the PM_{10} threshold of 50 $\mu g/m^3$ is computed on a daily basis for Piemonte region (Italy).

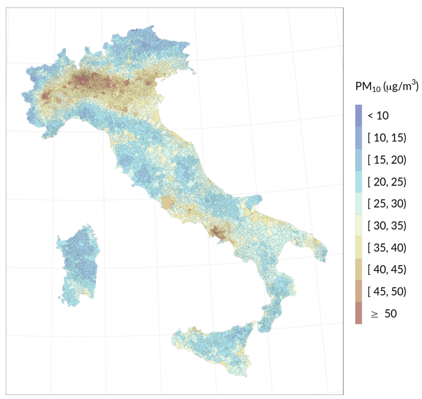

(a) Annual mean concentrations

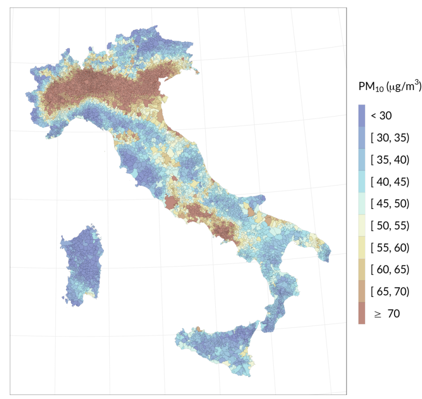

(b) Annual 90.4 percentile concentrations

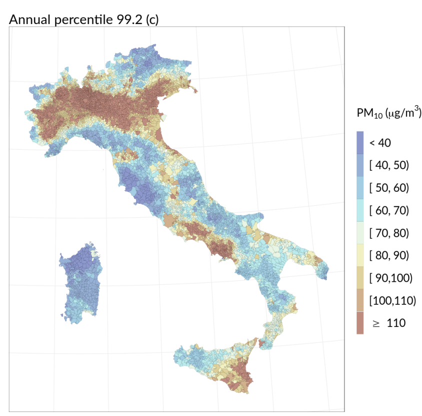

(c) Annual 99.2 percentile concentrations

Figure 9: Population exposure to PM_{10} concentrations. EU air quality limit value for PM_{10} daily concentrations is exceeded when 90.4 percentile is higher than 50 $\mu g/m^3$, while the more severe WHO air quality guideline is exceeded when 99.2 percentile is higher than 50 $\mu g/m^3$. The EU PM_{10} annual average limit value is 40 $\mu g/m^3$, while the WHO air quality guideline is 20 $\mu g/m^3$.

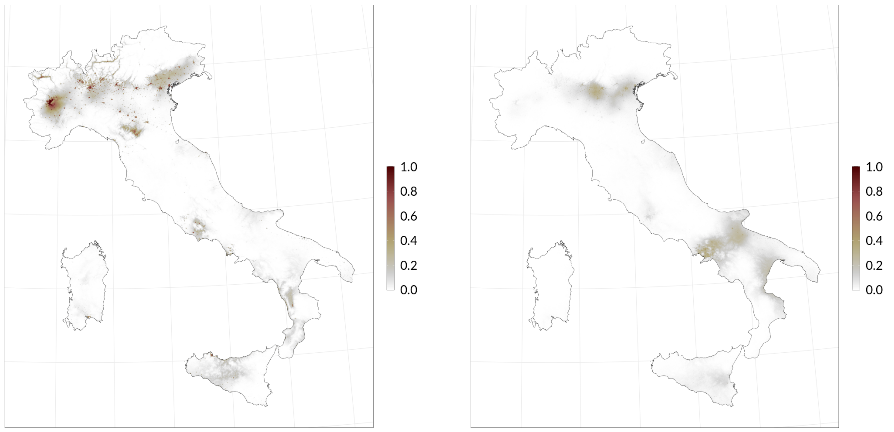

(a) January 26th

(b) July 21st

Figure 10: PM_{10} exceedance probabilities (probabilities of PM_{10} concentrations exceeding the threshold of 50 $\mu g/m^3$) for January 26th and July 21st, 2015.

POE maps represent a valid tool for those involved in managing the impacts of atmospheric pollution. The probability of exceeding a critical level in an area can be relevant both to increase public awareness in relation to air pollution, and to develop or improve mitigation actions on a local scale.

Based on the simulation results discussed in Section 3.3, we calculated, for each cell of the reference grid, the probabilities of exceeding the daily limit value of 50 $\mu g/m^3$ for PM_{10}. Specifically, the exceedance probability of each cell was calculated as the number of exceedances divided by the total number of simulations (1000).

The final maps are shown in Figure 10. For the selected winter day (January 26th), the Po Valley exhibits several areas with high probabilities of exceedence, whose spatial distribution (around the large urban agglomerations) resembles, not surprisingly, the spatial pattern of the high pollutant concentrations seen in Figure 7 a). Conversely, the POE map for July 21st is characterized by low probability values (below 0.4), in accordance with the fact that PM_{10} is not a critical pollutant in summer.

4. Conclusions

In this paper we proposed a Bayesian hierarchical spatio-temporal model for PM_{10} daily concentrations. The model was applied, separately for each month, to the PM_{10} concentrations measured during 2015 by the Italian monitoring network. This month-by-month approach represents an effective modeling solution for taking into account the seasonal variability of the phenomenon avoiding the use of a more complex year-based model which would require extremely higher computational costs. Moreover, with our modeling strategy it is possible to evaluate how the relationship between the considered predictors and PM_{10} concentrations change across months. To the best of our knowledge no studies have assessed the predictors effect on the monthly timescale. From our results, we obtained that the covariates with the most pronounced seasonal effect are temperature, Planet Boundary Layer at 00:00, altitude and impervious surface. A clear but less marked impact of AOD on the PM_{10} was also found. It is worthwhile to point out that originally our analysis considered a larger set of potential predictors, including those commonly used in PM modeling, such as the "weekend effect" or the Corine Land Cover land-use classification. However, most of them did not enter the final model because not statistically significant. Our final selection of predictors, including 11 variables, is supported by the analysis of the residuals of the models which appear to be uncorrelated both in space and time.

The main outcome of our model is the continuous (1km $\times$ 1km) PM_{10} map that we can estimate on a daily basis and is equipped with an uncertainty measure like the relative width of the posterior interquartile range. These high-resolution maps represent a fundamental tool for air quality management (at the national, regional and local level) with the aim of developing and monitoring programs and actions taken to improve air quality. As far as we know, there are very few other proposals in the statistical literature for this problem of mapping PM_{10} concentrations on a large domain like Italy with a fine grid. In this regard, it is worth mentioning Stafoggia et al. (2017) and Stafoggia et al.

(2019), which adopted LMM and a land-use random-forest model, respectively. Our opinion is that both the approaches are methodologically sound but they are implemented by adopting a very complex modeling pipeline starting from missing data imputation and ending with predictions improvement by using small-scale predictors connected with very local sources. This gives rise to a computationally expensive modeling solution and to a difficulty in quantifying properly the uncertainty of the final predictions by taking into account all the variability sources. We believe that our modeling strategy, which is simple in its formulation and implementation, could represent a valid solution for this challenging problem which has an important connection with environment and human health protection. We would like to point out that, starting from the daily PM_{10} maps, our modeling approach is also able to produce probability of exceedance and population-weighted exposure maps, that can be defined both at the grid or area level. While the former can be used to assess the compliance with air quality guidelines set for human health protection, the latter are necessary to link exposure to the health outcomes in epidemiological studies that investigate the long-term effect of air pollution exposure.

The computational complexity of our analysis, given by the fact that we work with a large dataset (ca. 400 monitoring stations) and a fine spatio-temporal grid of about 11 millions cells, is managed by using the INLA-SPDE approach for model estimation and prediction. The cross-validation results suggest a good predictive performance of the model at almost all concentration levels, with the correlation between observed and predicted values ranging from 0.71 (in July) and 0.91 (in February), and the bias in the range 0.22 (August) - 1.07 $\mu g/m^3$ (January). Despite these encouraging results, large deviations between modeled and high extreme PM_{10} observations remain an issue. This could be partly addressed in future work, for example, by improving the spatial resolution of the predictors (AOD and meteorological variables), including a quantitative description of the Saharan dust, or considering further sources of air pollution (fires, proximity to power plants, industrial facilities and so on). In this respect, the results of Schneider et al. (2020) suggest that future research developments should investigate how the use of gridded PM emissions products from reanalysis or chemical transport models can further improve the predictive model performance.

5. Acknowledgments

This research was partially funded by the Project "Piattaforma Tematica del Sentinel Collaborative GS per la Qualità dell'Aria". The agreement was signed between ASI (Agenzia Spaziale Italiana) and ISPRA (Istituto Superiore per la Protezione e Ricerca Ambientale). CUP: F82F17000000005.

References

Al-Hamdan, M. Z., Crosson, W. L., Limaye, A. S., Rickman, D. L., Quattrochi, M. G., D. A.and Estes Jr., Qualters, J. R., Sinclair, A. H., Tolsma, D. D., Adeniyi, K. A., & Niskar, A. S. (2009). Methods for characterizing fine particulate matter using ground observations and remotely sensed data: potential use for environmental public health surveillance. *J Air Waste Manag Assoc*, *59*, 865–881.

Attarchi, S. (2020). Extracting impervious surfaces from full polarimetric sar images in different urban areas. *Int J Remote Sens.*, *41*, 4644–4663.

Bakka, H., Rue, H., Fuglstad, G.-A., Riebler, A., Bolin, D., Illian, J., Krainski, E., Simpson, D., & Lindgren, F. (2018). Spatial modeling with `r-inla`: a review. *Wiley Interdiscip Rev Comput Stat.*, .

Barmpadimos, I., Keller, J., Oderbolz, D., Hueglin, C., & Prevot, A. S. H. (2012). One decade of parallel fine ($PM_{2.5}$) and coarse (PM_{10}–$PM_{2.5}$) particulate matter measurements in europe: trends and variability. *Atmospheric Chem. Phys.*, *12*, 3189–3203.

Barnaba, F., Bolignano, A., Di Liberto, L., Morelli, M., Lucarelli, F., Nava, S., Perrino, C., Canepari, S., Basart, S., Costabile, F., Dionisi, D., Ciampichetti, S., Sozzi, R., & Gobbi, G. P. (2017). Desert dust contribution to PM_{10} loads in italy: methods and recommendations addressing the relevant european commission guidelines in support to the air quality directive 2008/50. *Atmospheric Environ.*, *161*, 288–305.

Beloconi, A., Chrysoulakis, N., Lyapustin, A., Utzinger, J., & Vounatsou, P. (2018). Bayesian geostatistical modelling of PM_{10} and $PM_{2.5}$ surface level concentrations in europe using high-resolution satellite-derived products. *Environ. Int.*, *121*, 57–70.

Blangiardo, M., & Cameletti, M. (2015). *Spatial and spatio-temporal Bayesian models with* `r-inla`. Wiley.

Blangiardo, M., Cameletti, M., Baio, G., & Rue, H. (2013). Spatial and spatio-temporal models with `r-inla`. *Spat Spatiotemporal Epidemiol*, *4*, 33 – 49.

Blangiardo, M., Pirani, M., Kanapka, L., Hansell, A., & Fuller, G. (2019). A hierarchical modelling approach to assess multi pollutant effects in time-series studies. *PLOS ONE*, .

Cameletti, M., Ignaccolo, R., & Bande, S. (2011). Comparing spatio-temporal models for particulate matter in Piemonte. *Environmetrics*, *22*, 985–996.

Cameletti, M., Lindgren, F., & Simpson, D. (2013). Spatio-temporal modeling of particulate matter concentration through the SPDE approach. *Adv Stat Anal.*, *97*, 109–131.

Chu, H. J., Huang, B., & Lin, C. Y. (2015). Modeling the spatio-temporal heterogeneity in the PM_{10}-$PM_{2.5}$ relationship. *Atmospheric Environ.*, *102*, 176–182.

Clark, J. S., & Gelfand, A. E. (2006). *Hierarchical modelling for the environmental sciences*. Oxford University Press.

Cocchi, D., Greco, F., & Trivisano, C. (2007). Hierarchical space-time modelling of PM_{10} pollution. *Atmospheric Environ.*, *41*, 532–542.

Cohen, A. J., Brauer, M., Burnett, R., Anderson, H. R., Frostad, J., Estep, K., Balakrishnan, K., Brunekreef, B., Dandona, L., Dandona, R., Feigin, V., Freedman, G., Hubbell, B., Jobling, A., Kan, H., Knibbs, L., Liu, Y., Martin, R., Morawska, L., Pope, C. A., Shin, H., Straif, K., Shaddick, G., Thomas, M., van Dingenen, R., van Donkelaar, A., Vos, T., Murray, C. J. L., & Forouzanfar, M. H. (2017). Estimates and 25-year trends of the global burden of disease attributable to ambient air pollution: an analysis of data from the Global Burden of Diseases study 2015. *The Lancet*, *389*, 1907–1918.

Cressie, N. A. C., & Wikle, C. K. (2011). *Statistics for spatio-temporal data*. Wiley.

Danielson, J., & Gesch, D. (2011). *Global multi-resolution terrain elevation data 2010 (GMTED2010): U.S. Geo-logical Survey Open-File Report 2011–1073*. Technical Report Department of the Interior U.S. Geological Survey.

De Marco, C., Boselli, A., D'Anna, A., Perillo, G., Sannino, A., Sasso, G., Sirignano, M., Spinelli, N., & Wang, X. (2018). Coordinated multiparametric characterization of atmospheric particulate in the Campania region of Italy. *WIT Trans. Ecol. Environ.*, *230*, 619–630.

Denby, B., Dudek, A., Walker, S., Costa, A., Monteiro, A., van den Elshout, S., & Fisher, B. (2011). Towards uncertainty mapping in air-quality modelling and assessment. *Int J Environ Pollut.*, *44*, 14–23.

Di, Q., Kloog, I., Koutrakis, P., Lyapustin, A., Wang, Y., & Schwartz, J. (2016). Assessing $PM_{2.5}$ exposures with high spatiotemporal resolution across the continental United States. *Environ. Sci. Technol.*, *50*, 4712–4721.

EEA (2019). *Air quality in Europe: 2019 report*. Technical Report European Environment Agency Luxembourg.

EU (2001). Directive 2001/81/ec of the European Parliament and of the Council of 23 october 2001 on national emission ceilings for certain atmospheric pollutants. 27/11/2001.

EU (2002). *Guidance on Assessment under the EU Air Quality Directives*. Technical Report European Union.

EU (2008). Directive 2008/50/ec of the European Parliament and of the Council of 21 may 2008 on ambient air quality and cleaner air for Europe. 11/6/2008.

Forlani, C., Bhatt, S., Cameletti, M., Krainski, E., & Blangiardo, M. (2020). A joint Bayesian space–time model to integrate spatially misaligned air pollution data in r-inla. *Environmetrics*, .

Fuglstad, G.-A., Simpson, D. P., Lindgren, F., & Rue, H. (2019). Constructing priors that penalize the complexity of Gaussian Random Fields. *J. Am. Stat. Assoc.*, *114*, 445–452.

Galecki, A., & Burzykowski, T. (2013). *Linear Mixed-Effects Models using R*. Springer.

Gilks, W., Richardson, S., & Spiegelhalter, D. (1995). *Markov Chain Monte Carlo in practice*. Chapman and Hall/CRC.

Gòmez-Rubio, V. (2020). *Bayesian inference with INLA*. CRC Press.

Grange, S. K., Carslaw, D. C., Lewis, A. C., Boleti, E., & Hueglin, C. (2018). Random Forest meteorological normalisation models for Swiss PM_{10} trend analysis. *Atmospheric Chem. Phys.*, *18*, 6223–6238.

Grisotto, L., Consonni, D., Cecconi, L., Catelan, D., Lagazio, C., Bertazzi, P. B., Baccini, M., & Biggeri, A. (2016). Geostatistical integration and uncertainty in pollutant concentration surface under preferantial sampling. *Geospat Health*, *11*, 56–61.

Haklay, M. M., Basiouka, S., Antoniou, V., & Ather, A. (2010). How many volunteers does it take to map an area well? The validity of Linus' law to volunteered geographic information. *Cartogr J.*, *47*, 315–322.

Heaton, M. J., Datta, A., Finley, A. O., Furrer, R., Guinness, J., Guhaniyogi, R., Gerber, F., Gramacy, R. B., Hammerling, D., Katzfuss, M., Lindgren, F., Nychka, D. W., Sun, F., & Zammit-Mangion, A. (2019). A case study competition among methods for analyzing large spatial data. *J Agric Biol Environ Stat*, *24*, 398–425.

Hersbach, H., Bell, B., Berrisford, P., Hirahara, S., Horányi, A., Muñoz-Sabater, J., Nicolas, J., Peubey, C., Radu, R., Schepers, D., Simmons, A., Soci, C., Abdalla, S., Abellan, X., Balsamo, G., Bechtold, P., Biavati, G., Bidlot, J., Bonavita, M., De Chiara, G., Dahlgren, P., Dee, D., Diamantakis, R., M.and Dragani, Flemming, J., Forbes, R., Fuentes, M., Geer, A., Haimberger, L., Healy, S., Hogan, R., Hólm, E., Janisková, M., Keeley, S., Laloyaux, P., Lopez, P., Lupu, C., Radnoti, G., de Rosnay, P., Rozum, I., Vamborg, F., Villaume, S., & Thépaut, J. (2020). The ERA5 Global Reanalysis. *Q J R Meteorol Soc*, .

Hidy, G. M., Brook, J. R., Chow, J. C., Green, M., Husar, R. B., Lee, C., Scheffe, R. D., Swanson, A., & Watson, J. G. (2009). Remote sensing of particulate pollution from space: Have we reached the promised land? *J Air Waste Manag Assoc.*, *59*, 1130–1139.

Hoek, G. (2017). Methods for assessing long-term exposures to outdoor air pollutants. *Curr. Environ. health Rep.*, *4*, 450–462.

Huang, G. ., Lee, D., & Scott, E. M. (2018). Multivariate space-time modelling of multiple air pollutants and their health effects accounting for exposure uncertainty. *Stat Med.*, *37*, 1134–1148.

ISPRA (2019). *Analisi dei trend dei principali inquinanti atmosferici in Italia (2008-2017)*. Technical Report ISPRA Roma.

ISPRA (2020). *Annuario dei Dati Ambientali - Edizione 2019*. Technical Report Istituto Superiore per la Protezione e la Ricerca Ambientale.

Kloog, I., Sorek-Hamera, M., Lyapustin, A., Coull, B., Wange, Y., Just, A., Schwartz, J., & Broday, D. (2015). Estimating daily $PM_{2.5}$ and PM_{10} across the complex geo-climate region of Israel using MAIAC satellite-based aod data. *Atmospheric Environ.*, *122*, 409–416.

Langanke, T. (2015). *Outdoor Air Pollution. IARC monographs on the evaluation of carcinogenic risk to humans.*. Technical Report International Agency for Research on Cancer.

Langanke, T. (2018). *Copernicus Land Monitoring Service – High Resolution Layer Imperviousness: Product Specifications Document*. Technical Report EEA.

Lindgren, F., Rue, H., & Lindström, J. (2011). An explicit link between Gaussian Fields and Gaussian Markov Random Fields: the Stochastic Partial Differential Equation approach. *J. Royal Stat. Soc.: Series B (Statistical Methodology)*, *73*, 423–498.

Liu, Y., Guoa, H., Mao, G., & Yang, P. (2008). A Bayesian hierarchical model for urban air quality prediction under uncertainty. *Atmospheric Environ.*, *42*, 8464–8469.

Lyapustin, Y., A.and Wang, Korkin, S., & Huang, D. (2018). Modis collection 6 maiac algorithm. *Atmos Meas Tech.*, *11*, 5741–5765.

Martuzzi, M., Mitis, F., Iavarone, I., & Serinelli, M. (2006). *Health impact of PM_{10} and Ozone in 13 Italian cities*. Technical Report World Health Organization Regional Office for Europe.

Matassoni, L., Pratesi, G., Centioli, D., Cadoni, F., Malesani, P., Caricchia, A. M., & Di Bucchianico, A. M. (2009). Saharan dust episodes in Italy: influence on PM_{10} daily limit value (DLV) exceedances and the related synoptic. *Environ. Sci. Process. Impact*, *11*, 1586–1594.

Ott, R. W. (1990). A physical explanation of the lognormality of pollutant concentrations. *J Air Waste Manag Assoc*, *40*, 1378–1383.

Pérez, C., Haustein, K., Janjic, Z., Jorba, O., Huneeus, N., Baldasano, J. M., Black, T., Basart, S., Nickovic, S., Miller, R. L., Perlwitz, J. P., Schulz, M., & Thomson, M. (2011). Atmospheric dust modeling from meso to global scales with the online NMMB/BSC-Dust model; Part 1: model description, annual simulations and evaluation. *Atmospheric Chem. Phys.*, *11*, 13001–13027.

Perrino, C., Catrambone, M., & Canepari, S. (2020). Chemical composition of PM_{10} in 16 urban, industrial and background sites in Italy. *Atmosphere*, *11*.

Pey, J., Querol, X., Alastuey, A., Forastiere, F., & Stafoggia, M. (2013). African dust outbreaks over the Mediterranean Basin during 2001–2011: PM_{10} concentrations, phenomenology and trends, and its relation with synoptic and mesoscale meteorology. *Atmospheric Chem. Phys.*, *13*, 1395–1410.

Pikridas, M., Vrekoussis, M., Sciare, J., Kleanthous, S., Vasiliadou, E., Kizas, C., Savvides, C., & Mihalopoulos, N. (2018). Spatial and temporal (short and long term) variability of submicron, fine and sub-10 μm particulate matter (PM_1, $PM_{2.5}$, PM_{10}) in Cyprus. *Atmospheric Environ.*, *191*, 79–93.

Pinheiro, J., Bates, D., DebRoy, S., Sarkar, D., & R Core Team (2020). *nlme: Linear and Nonlinear Mixed Effects Models*. R package version 3.1-148.

Pirani, M., Gulliver, J., Fuller, G. W., & Blangiardo, M. (2014). Bayesian spatiotemporal modelling for the assessment of short-term exposure to particle pollution in urban areas. *J. Expo. Sci. Environ. Epidemiol.*, *24*, 319–327.

Piscitelli, P., Valenzano, B., Rizzo, E., Maggiotto, G., Rivezzi, M., Corcione, F. E., & Miani, A. (2019). Air pollution and estimated health costs related to road transportations of goods in Italy: A first healthcare burden assessment. *Int. J. Environ. Res. Public Health*, *16*.

Plummer, M. (2016). rjags: Bayesian graphical models using MCMC. R package version 4-6.

Pollice, A., & Jona Lasinio, G. (2010). Spatio temporal analysis of the PM_{10} concentration over the Taranto area. *Environ. Monit. Assess.*, *162*, 177–190.

Porcu, E., Montero, J., & Schlather, M. (2012). *Advances and Challenges in Space-time Modelling of Natural Events*.

R Core Team (2018). *R: A Language and Environment for Statistical Computing*. R Foundation for Statistical Computing Vienna, Austria. URL: `www.R-project.org`.

Raffaelli, K., Deserti, M., Stortini, M., Amorati, R., Vasconi, M., & Giovannini, G. (2020). Improving air quality in the Po Valley, Italy: some results by the LIFE-IP-PREPAIR project. *Atmosphere*, *11*.

Rue, H., & Held, L. (2005). *Gaussian Markov Random Fields: theory and applications*. Chapman & Hall/CRC Monographs on Statistics & Applied Probability. CRC Press.

Rue, H., Martino, S., & Chopin, N. (2009). Approximate Bayesian inference for latent Gaussian models using integrated nested Laplace approximations (with discussion). *J. Royal Stat. Soc., Series B*, *71*, 319–392.

Sahu, S. K. (2011). Hierarchical Bayesian models for space-time air pollution data. *Handbook of Statistics*, *30*, 477–495.

Samoli, E., Stafoggia, M., Rodopoulou, S., Ostro, B., Declercq, C., Alessandrini, E., Díaz, J., Karanasiou, A., Kelessis, A. G., Le Tertre, A., Pandolfi, P., Randi, G., Scarinzi, C., Zauli-Sajani, S., Katsouyanni, K., Forastiere, F., & the MED-PARTICLES Study group. (2013). Associations between fine and coarse particles and mortality in Mediterranean cities: Results from the MED-PARTICLES project. *Environ. Health Perspect.*, *121*.

Sarafian, R., Kloog, I., Just, A. C., & Rosenblatt, J. D. (2019). Gaussian Markov Random Fields versus Linear Mixed Models for satellite-based $PM_{2.5}$ assessment: evidence from the Northeastern USA. *Atmospheric Environ.*, *205*, 30–35.

Schneider, R., Vicedo-Cabrera, A. M., Sera, F., Masselot, P., Stafoggia, M., de Hoogh, K., Kloog, I., Reis, S., Vieno, M., & Gasparrini, A. (2020). A satellite-based spatio-temporal machine learning model to reconstruct daily $PM_{2.5}$ concentrations across Great Britain. *Remote Sens.*, *12*.

Segura, S., Estellés, V., Utrillas, M. P., & Martínez-Lozano, J. (2017). Long term analysis of the columnar and surface aerosol relationship at an urban European coastal site. *Atmospheric Environ.*, *167*, 309–322.

Shaddick, G., Thomas, M. L., Green, A., Brauer, M., van Donkelaar, A., Burnett, R., Chang, H. H., Cohen, A., van Dingenen, R., Dora, C., Gumy, S., Liu, Y., Martin, R., Waller, L. A., West, J., & Zidek, J. V. (2017). Data integration model for air quality: a hierarchical approach to the global estimation of exposures to ambient air pollution. *J. Royal Stat. Soc.: Series C (Applied Statistics)*, *67*, 231–253.

Shahraiyni, H. T., & Sodoudi, S. (2016). Statistical modeling approaches for PM_{10} prediction in urban areas; a review of 21st-century studies. *Atmosphere*, *7*.

Sheppard, L., Slaughter, J., Schildcrout, J., L-J Sally Liu, L.-J. S., & Lumley, T. (2005). Exposure and measurement contributions to estimates of acute air pollution effects. *J. Expo. Sci. Environ. Epidemiol.*, *15*, 366–376.

Shi, Y., Hu, F., Xiao, Z., Fan, G., & Zhang, Z. (2020). Comparison of four different types of planetary boundary layer heights during a haze episode in Beijing. *Sci. Total Environ.*, *711*.

Simpson, D. P., Rue, H., Riebler, A., Martins, T. G., & Sørbye, S. H. (2017). Penalising model component complexity: a principled, practical approach to constructing priors. *Stat. Sci.*, *32*, 1–28.

Spiegelhalter, D. J., Thomas, A., Best, N. G., & Gilks, W. R. (1995). Bugs: Bayesian inference using gibbs sampling. version 0.50.

Stafoggia, M., Bellander, T., Bucci, S., Davoli, M., de Hoogh, K., de' Donato, F., Gariazzo, C., Lyapustin, A., Michelozzi, P., Renzi, M., Scortichini, M., Shtein, A., Viegi, G., Kloog, I., & Schwartz, J. (2019). Estimation of daily PM_{10}–$PM_{2.5}$ concentrations in Italy, 2013-2015, using a spatiotemporal land-use Random-forest model. *Environ. Int.*, *124*, 170 – 179.

Stafoggia, M., Schwartz, J., Badaloni, C., Bellander, T., Alessandrini, E., Cattani, G., De'Donato, F., Gaeta, A., Leone, G., Lyapustin, A., Sorek-Hamer, M., de Hoogh, K., Di, Q., Forastiere, F., & Kloog, I. (2017). Estimation of daily PM_{10} concentrations in italy (2006–2012) using finely resolved satellite data, land use variables and meteorology. *Environ. Int.*, *99*, 234–244.

Stein, A. F., Draxler, R. R., Rolph, G. D., Stunder, B. J. B., Cohen, M. D., & Ngan, F. (2015). NOAA's HYSPLIT atmospheric transport and dispersion modeling system. *Bull Am Meteorol Soc*, *96*, 2059–2077.

Strobl, C. (2008). Postgis. In *Encyclopedia of GIS* (p. 891–898). Boston, MA: Springer US.

Sørbye, S. H., & Rue, H. (2017). Penalised complexity priors for stationary autoregressive processes. *J Time Ser Anal*, *38*, 923–935.

Team, S. D. (2015). Stan modeling language user's guide and reference manual. version 2.6.1.

Tobías, A., Pérez, L., Díaz, J., Linares, C., Pey, J., Alastruey, A., & Querol, X. (2011). Short-term effects of particulate matter on total mortality during saharan dust outbreaks: a case crossover analysis in Madrid (Spain). *Sci. Total Environ.*, *412-413*, 386–389.

Warsono, K. P. S., Bartolucci, A. A., & Bae, S. (2001). Mathematical modeling of environmental data. *Math Comput Model.*, *33*, 793–800.

Weber, S. A., Engel-Cox, J. A., Hoff, R. M., Prados, A. I., & Zhang, H. (2010). An improved method for estimating surface fine particle concentrations using seasonally adjusted satellite aerosol optical depth. *J Air Waste Manag Assoc.* ,, *60*, 574–585.

WHO (2013). *Review of evidence on health aspects of air pollution – REVIHAAP Project*. Technical Report World Health Organization.

Yang, Y., Christakos, G., Huang, W., Lin, C., Fu, P., & Mei, Y. (2016). Uncertainty assessment of $PM_{2.5}$ contamination mapping using spatiotemporal sequential indicator simulations and multi-temporal monitoring data. *Sci Rep*, *6*.

Yuan, Y., Bachl, F. E., Finn, L., Borchers, D. L., Illian, J. B., Buckland, S. T., Rue, H., & Gerrodette, T. (2017). Point process models for spatio-temporal distance sampling data from a large-scale survey of blue whales. *Ann. Appl. Stat.*, *11*, 2270–2297.

Zhang, J., Li, B., Chen, Y., Chen, M., Fang, T., & Liu, Y. (2018). Eigenvector spatial filtering regression modeling of ground $PM_{2.5}$ concentrations using remotely sensed data. *Int. J. Environ. Res. Public Health*, *15*.

Zou, B., Wilson, J. G., Zhan, F. B., & Zeng, Y. (2009). Air pollution exposure assessment methods utilized in epidemiological studies. *Environ. Sci. Process. Impact*, *11*, 475–490.